Potential Impact of the Eurasian Boreal Forest on North Pacific Climate Variability*

MICHAEL NOTARO AND ZHENGYU LIU

Center for Climatic Research, University of Wisconsin—Madison, Madison, Wisconsin

(Manuscript received 21 February 2006, in final form 3 August 2006)

ABSTRACT

The authors demonstrate that variability in vegetation cover can potentially influence oceanic variability through the atmospheric bridge. Experiments aimed at isolating the impact of variability in forest cover along the poleward side of the Asian boreal forest on North Pacific SSTs are performed using the fully coupled model, Fast Ocean Atmosphere Model–Lund Potsdam Jena (FOAM-LPJ), with dynamic atmosphere, ocean, and vegetation. The northern edge of the simulated Asian boreal forest is characterized by substantial variability in annual forest cover, with an east–west dipole pattern marking its first EOF mode. Simulations in which vegetation cover is allowed to vary over north/central Russia exhibit statistically significant greater SST variance over the Kuroshio Extension. Anomalously high forest cover over North Asia supports a lower surface albedo with higher temperatures and lower sea level pressure, leading to a reduction in cold advection into northern China and in turn a decrease in cold air transport into the Kuroshio Extension region. Variability in the large-scale circulation pattern is indirectly impacted by the aforementioned vegetation feedback, including the enhancement in upper-level jet wind variability along the north–south flanks of the East Asian jet stream.

1. Introduction

Numerous modeling studies have indicated that vegetation can substantially impact the atmosphere, both locally and remotely. Fully coupled climate models have shown that vegetation's influence on the atmosphere is established through biophysical feedbacks involving surface albedo (energy), evapotranspiration (moisture), and surface roughness (momentum). Within the boreal forests, the vegetation albedo feedback appears to be critical, particularly when the forest canopy masks the underlying snow cover (Robinson and Kukla 1985; Bonan et al. 1992; Betts and Ball 1997; Bonan 2002). Modeling experiments in which the global boreal forests were replaced by bare ground or tundra (Bonan et al. 1992; Snyder et al. 2004) attest to the widespread influence of the boreal forest on temperature. Bonan et al. (1992) concluded that the resulting cooling was greatest in April and extended remotely even into the subtropics.

Field measurements have likewise revealed that Arctic forest and tundra have significantly different impacts on the local climate. Compared to tundra, the boreal forest is typically characterized by a lower surface albedo (Chapin et al. 2000; Beringer et al. 2005; Lundberg and Beringer 2005), higher temperature (Beringer et al. 2005), lower atmospheric moisture (Beringer et al. 2005), lower evaporative fluxes (Shaeffer and Reiter 1987; Riseborough and Burn 1988; Bowers and Bailey 1989; Isard and Belding 1989; Rouse et al. 1992), and higher Bowen ratio (Lafleur and Rouse 1995; Beringer et al. 2005). Along the boreal forest–tundra boundary, vegetation changes alter the surface albedo and roughness (Chapin et al. 2000), resulting in changes in surface energy exchange (Bonan et al. 1992; Chapin et al. 2000; Lloyd 2005). Compared to nonvegetated Arctic surfaces, shrublands actually support a deeper snowpack by reducing near-surface wind speeds and thereby reducing wind-driven sublimation; this likely encourages increased springtime runoff, higher winter soil temperatures, and reduced wintertime sensible heat loss (McFadden 1998; Sturm et al. 2001).

Two recent studies (Liu et al. 2006; Notaro et al. 2006) have attempted to statistically quantify observed vegetation feedbacks. These studies support the findings of previous modeling studies that high-latitude forests induce a strong positive feedback on temperature. For example, Liu et al. (2006) noted a significant positive forcing of observed summer–autumn fraction of

* Center for Climatic Research Contribution Number 904.

Corresponding author address: Dr. Michael Notaro, Center for Climatic Research, University of Wisconsin—Madison, 1225 West Dayton Street, Madison, WI 53706.
E-mail: mnotaro@wisc.edu

DOI: 10.1175/JCLI4052.1

photosynthetically active radiation (FPAR) on October temperatures across eastern Siberia. Liu et al. (2006) also showed that Fast Ocean Atmosphere Model–Lund Potsdam Jena (FOAM-LPJ) produced a positive vegetation forcing on temperature across North Asia that agreed with the observed feedback estimates.

The complex impacts of vegetation variability on atmospheric variability have been explored in a few modeling studies. Zeng et al. (1999) and Delire et al. (2004) found that interactive vegetation led to enhanced precipitation variability at lower frequencies and reduced variability at higher frequencies. Zeng et al. (2002) also concluded that positive feedbacks from interactive vegetation can produce spatial changes in vegetation and rainfall gradients, particularly over Africa.

The possibility that vegetation variability might impact oceanic climate variability remains largely unexplored. For instance, vegetation cover variations likely produce local responses in temperature with the potential for remote atmospheric and oceanic responses. Wohlfahrt et al. (2004) identified a synergy between oceanic and vegetation feedbacks that amplified their simulated climatic change. The interannual variability of SST supports a smoother desert–forest transition, such as in the Sahel (Zeng and Neelin 2000). To study the impact of vegetation variability on oceanic variability, it is necessary to apply a GCM with both dynamic vegetation and ocean, such as FOAM-LPJ.

We will investigate the impact of variability in forest cover along the poleward side of the North Asian boreal forest on North Pacific SST variability using the fully coupled model, FOAM-LPJ. This study is the first to demonstrate the simulated response of SSTs to vegetation variability in a fully coupled atmosphere–ocean–vegetation GCM. We select the area of the northern Asian boreal forest due to its substantial forest cover variability and potent albedo feedbacks within the control simulation and perform a set of experiments aimed at isolating the impact of vegetation variability within the region. Section 2 describes the model and experiments. Section 3 discusses the mean and variance of simulated vegetation and compares the results with satellite observations. The impact of North Asian vegetation variability on Pacific SSTs and the atmosphere is presented in sections 4 and 5, respectively. A mechanism for this remote feedback is proposed in section 6. Finally, the conclusions are given in section 7.

2. Model

a. Model description

Simulations are performed using FOAM-LPJ, which is a fully coupled global atmosphere–ocean–land model with dynamic vegetation (Gallimore et al. 2005; Notaro et al. 2005). The coupled atmospheric–oceanic component is the FOAM version 1.5 (Jacob 1997). The atmospheric component is a fully parallel version of the National Center for Atmospheric Research's (NCAR) Community Climate Model (CCM2; Drake et al. 1995), which has been updated with CCM3 atmospheric physics (Kiehl et al. 1998). The atmosphere is simulated with a horizontal resolution of R15 (approximately $4.5° \times 7.5°$) and 18 vertical levels. The oceanic component, Ocean Model Version 3 (OM3), is a finite-difference, z-coordinate ocean model; it uses a horizontal resolution of $1.4° \times 2.8°$, 24 vertical levels, and an explicit free surface. FOAM uses the thermodynamic sea ice component model from Climate System Model version 1 (CSM1), NCAR's CSM Sea Ice Model (CSIM) version 2.26, but does not include sea ice dynamics. The sea ice model, which is driven by heat, momentum, and freshwater fluxes, includes lateral ice growth and melt in leads, snow on ice, and the production of brine pockets due to penetrating solar radiation.

FOAM is synchronously coupled to a modified version of the LPJ-dynamical global vegetation model (DGVM) (Sitch 2000; Cramer et al. 2001; McGuire et al. 2001; Sitch et al. 2003). The land grid has a horizontal resolution of $1.4° \times 2.8°$. The simulated nine plant function types (PFTs) consist of two tropical trees, three temperate trees, two boreal trees, and two grasses. FOAM-LPJ's vegetation processes include plant competition, biomass allocation, establishment, mortality, soil and litter biogeochemistry, natural fire, and successional vegetation changes. No relaxation or correction of climate forcing toward observations is applied to adjust the simulated vegetation. The original LPJ daily evapotranspiration process is modified in FOAM-LPJ to allow for diurnal calculations of soil temperature (Gallimore et al. 2005). The LPJ tree survival mechanism is also modified to permit less abrupt tree kill under extreme cold conditions (Gallimore et al. 2005). FOAM-LPJ has been applied to study the mid-Holocene (Gallimore et al. 2005), preindustrial to modern period (Notaro et al. 2005), and the twenty-first and twenty-second centuries (out to $4\times CO_2$) (Notaro et al. 2007).

Even without the use of flux adjustment, FOAM captures most of the major features of the observed climate as in most state-of-the-art climate models (Jacob 1997; Liu et al. 2003). It produces reasonable climate variability, including ENSO (Liu et al. 2000; Liu and Wu 2004), Pacific decadal variability (Wu et al. 2003; Wu and Liu 2003), and tropical Atlantic variability (Wu and Liu 2002), although the simulated variability is generally weaker than observed. Its simulated mean climate

TABLE 1. List of FOAM-LPJ simulations and whether or not annual vegetation cover is fixed or interactive over North Asia and the rest of the globe.

Simulation	North Asia	Rest of globe
INTVEG	Interactive	Interactive
NASIAFIX	Fixed	Interactive
NASIAINT	Interactive	Fixed
FIXVEG	Fixed	Fixed

and variability are comparable with higher-resolution models (Marshall et al. 2006a,b, manuscripts submitted to *Climate Dyn.*). The simulated biome distribution was found by Notaro et al. (2005) and Gallimore et al. (2005) to be in reasonable agreement with potential natural vegetation distribution.

b. Simulations

Four simulations are produced using FOAM-LPJ, each 400 yr in length (Table 1). Simulation INTVEG includes interactive vegetation globally, as opposed to simulation FIXVEG, which has fixed annual vegetation cover globally. In FIXVEG, the daily processes of LPJ coupling are permitted while the annual part of the coupling, which determines PFT fractional coverage, is turned off (Gallimore et al. 2005). The PFT distribution in the initial restart file is replaced by the mean coverage from the INTVEG control run and held constant throughout the simulation. Variations in seasonal leaf cover (phenology) are permitted in FIXVEG.

Two specialized simulations are produced, NASIAFIX and NASIAINT. In simulation NASIAFIX, annual vegetation cover is fixed over northern Asia (55°–80°N, 50°–140°E) but dynamically varying across the rest of the globe. In simulation NASIAINT, annual vegetation cover is fixed everywhere except interactive over northern Asia. By comparing simulations INTVEG to NASIAFIX or NASIAINT to FIXVEG, the simulated impact of variability in vegetation cover over northern Asia on the climate system can be assessed. The results are generally robust between both comparisons, so the INTVEG–NASIAFIX comparison is the only one presented in certain sections of the paper.

Several observational datasets are used to evaluate the model simulations. Satellite-based vegetation data include the Continuous Fields of Vegetation Cover dataset (DeFries et al. 1999, 2000) and the fractional vegetation cover (trees+grass) dataset (Zeng et al. 2000) for 1982–2000. Observed SST datasets include extended reconstructed SST (ERSST) (Smith and Reynolds 2003, 2004) and Kaplan extended SST (Kaplan et al. 1998; Parker et al. 1994; Reynolds and Smith 1994) datasets.

3. Simulated vegetation

Across Eurasia, three PFTs characterize the majority of the simulated vegetation cover: boreal needleleaf summergreen trees, boreal needleleaf evergreen trees, and C3 grasses. The simulated boreal forest is primarily comprised of a band of needleleaf summergreen trees across 50°–70°N, over south/central Russia and into northeast China. The model also produces an extensive, but less dense, forested region with boreal needleleaf evergreens over central/northern China and Mongolia. Boreal summergreen trees are more abundant at higher latitudes largely due to their hardiness as specified in LPJ, with no bioclimatic limit regarding the minimum coldest month mean temperature and less required growing degree-days than with the boreal needleleaf evergreen trees. Northern Asia, between 60° and 70°N, is moderately vegetated with C3 grasses and summergreen trees along the northern boreal forest. The total simulated forest cover in simulation INTVEG is shown in Fig. 1a. The region of moderate forest cover along the northern boreal forest is the focus of this paper.

The simulated vegetation cover is evaluated against the satellite-based Continuous Fields of Vegetation Cover dataset (not shown). The simulated boreal evergreen forest around 60°N closely matches its observed location. The model overproduces forest cover across Eurasia, largely due to a persistent wet bias. Within the central boreal forest and over China and Europe, simulated percent forest cover exceeds 90%. The model cold bias also expands the area of tundra and polar desert. Despite these biases, the simulated vegetation cover reasonably agrees with the observations, considering the lack of flux adjustment. Note that some differences between the simulated and satellite-derived vegetation cover can be attributed to the absence of land use and the categorization of shrubs as trees in the model. A further statistical analysis of feedbacks in FOAM-LPJ shows that the simulated vegetation feedbacks over Eurasia are largely consistent with statistical estimates based on remote sensing data (Liu et al. 2006).

Previous studies have demonstrated LPJ's success in simulating tundra vegetation (Sitch et al. 2003) and have shown that its simulated dynamics for tundra and boreal forest, particularly regarding succession and postdisturbance vegetation recovery, agree with observations (Bonan et al. 2003). Although LPJ lacks a shrub PFT, FOAM-LPJ produces short trees with shallow roots across the boreal tundra transition zone that are basically representative of observed shrubs.

The variance in annual forest cover from simulation INTVEG is shown in Fig. 1b. Globally, the most exten-

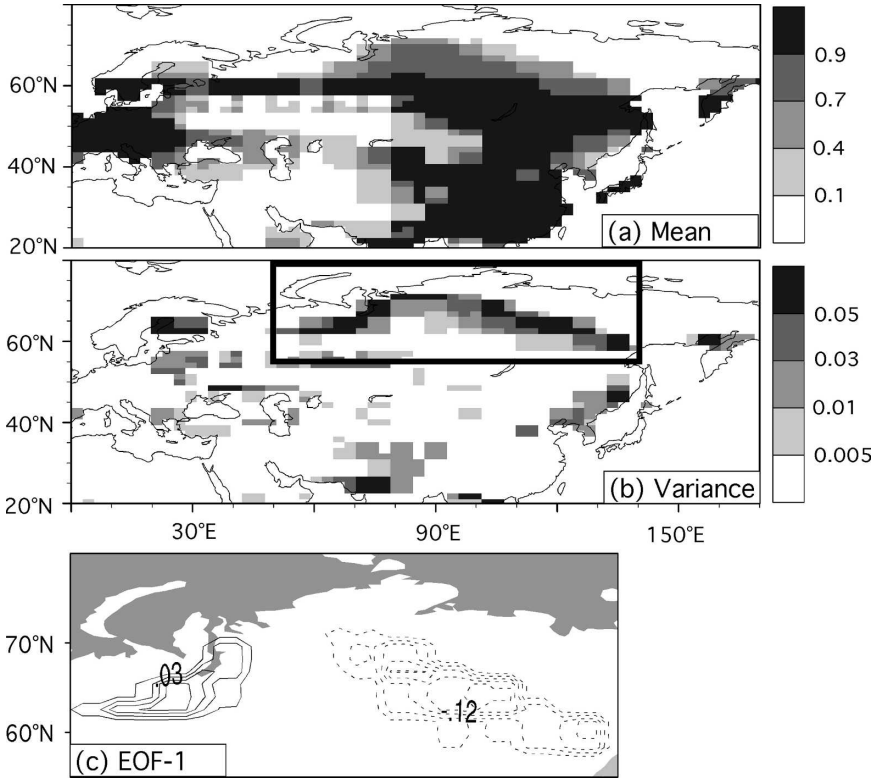

FIG. 1. (a) Mean forest cover fraction over north-central Asia from the 400-yr INTVEG simulation. The model simulates only natural vegetation and does not separate shrubs from trees. (b) Variance in annual forest cover fraction from the INTVEG simulation. The box indicates the area of fixed (interactive) vegetation cover in the NASIAFIX (NASIAINT) simulation. (c) Unrotated EOF-1 of annual forest cover fraction over North Asia from simulation INTVEG. The percent explained variance is 29% for EOF-1.

sive area of simulated forest cover variability is found over North Asia, along the northern edge of the boreal forest. The simulated forest cover over North Asia generally has a memory, or persistence time, in excess of one decade, based on the significance of lagged autocorrelations. This climatically sensitive region, as identified in Fig. 1b, lies within 55°–80°N, 50°–140°E (north-central Russia), and is characterized by a mix of boreal summergreen trees and C3 grasses. The lack of availability of long-term observed annual forest cover data, unfortunately, prevents a direct comparison against observations. However, there is a similar band of relatively high variance in observed fractional vegetation cover (tree+grass) during 1982–2000 over northern Asia within 60°–75°N, although less than the simulated variance. Since satellite data are only available for about two decades, it is not feasible to evaluate the simulated forest cover variability, which exhibits a decadal peak in variance. The boxed area in Fig. 1b represents the region of varying vegetation in NASIAINT and fixed vegetation in NASIAFIX. Based on unrotated EOF analysis of annual forest cover across northern Asia in simulation INTVEG, this area of relatively high forest cover variance is characterized by an east–west dipole pattern (Fig. 1c). The dipole pattern is mode 1 of the EOF analysis, explaining 29% of the variance. It can be described as a zonal oscillation of the northern boreal forest on a decadal time scale. The western (65.4°N, 119.5°E) and eastern (64.0°N, 66.1°E) dipole centers have a very similar mean fractional forest cover (0.47 and 0.45, respectively) and identical standard deviations of fractional forest cover (0.26), with a substantial negative correlation of -0.48 between the two locations' annual forest cover ($p < 0.1$). A further analysis suggests that this dipole in vegetation cover variability is forced by variability in the atmospheric circulation. An intensified Siberian high generates anomalous warming to the west and cooling to the east, enhancing forest cover to the west and suppressing forest cover to the east.

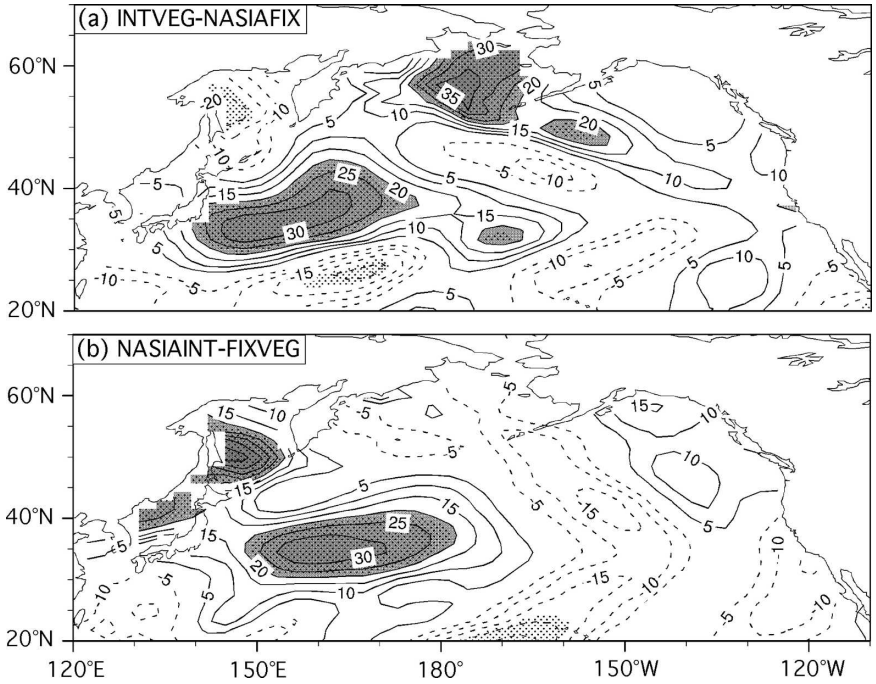

FIG. 2. Percent difference in annual SST variance between simulations (a) INTVEG and NASIAFIX and between (b) NASIAINT and FIXVEG. Dotted pattern indicates 90% significance from the F test. In both figures, the Kuroshio SST variance is increased by approximately 30% due to interactive vegetation cover over North Asia.

4. Impact of vegetation variability on ocean temperatures

Annual North Pacific SSTs from INTVEG are compared to observed SSTs (not shown) from both the ERSST and Kaplan extended SST datasets. Despite a persistent cold bias, the model produces a reasonable meridional gradient of annual SSTs over the North Pacific, including a tight gradient in the highly baroclinic Kuroshio Extension region. The model and observations exhibit a peak in SST variance in the Kuroshio Extension and the Gulf of Alaska, although the model's variance in the latter region is excessive due to too much sea ice variability there. The Pacific decadal oscillation (PDO) pattern appears as EOF-1 in both the INTVEG simulation and observations, with opposite signs between the west-central Pacific SSTs around 40°N and SSTs along the west coast of North America. The percent explained variance of EOF-1 is 33% in the Kaplan dataset and 44% in INTVEG. We conclude that FOAM-LPJ produces acceptable North Pacific SST variability, as previously determined by Wu et al. (2003) and Wu and Liu (2003).

On interannual and decadal time scales, the Kuroshio Extension exhibits the largest variability in sea surface and subsurface temperatures across the North Pacific (Miller et al. 1998; Xie et al. 2000). It is also characterized by the largest heat exchanges between the ocean and atmosphere across the extratropical North Pacific (Vivier et al. 2002). The Kuroshio Extension is a critical center for the PDO (Mantua et al. 1997; Kwon and Deser 2007). We find that variability in North Asian forest cover can potentially impose a significant impact on variability in the Kuroshio Extension.

The percent difference in variance of annual North Pacific SST is shown between INTVEG and NASIAFIX in Fig. 2a and between NASIAINT and FIXVEG in Fig. 2b. In both comparisons, the simulation with interactive vegetation cover over northern Asia (INTVEG and NASIAINT) is characterized by approximately 30% greater SST variance over the Kuroshio Extension, east of Japan ($p < 0.1$). The simulated vegetation cover over the northern boreal forest of Eurasia is therefore exhibiting a remote feedback on the Kuroshio SST. This SST variance enhancement over the Kuroshio Extension (30°–40°N, 140°E–180°) is most distinct in March–May (MAM) and June–August (JJA), with 37% ($p < 0.1$) greater variance in MAM and 31% ($p < 0.1$) greater in JJA, when comparing INTVEG with NASIAFIX.

Differences in the variance of annual ocean heat content within the top 100 m are analyzed between

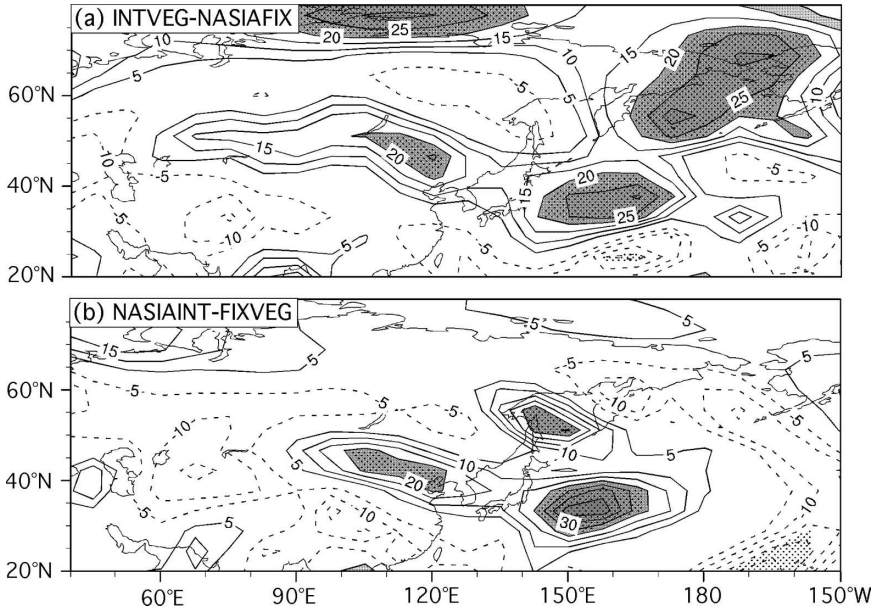

FIG. 3. Percent difference in annual surface air temperature variance between simulations (a) INTVEG and NASIAFIX and between (b) NASIAINT and FIXVEG. Dotted pattern indicates 90% significance from the F test. In both (a) and (b), the surface air temperature variance is increased by 20%–30% over the Kuroshio Extension and northeastern China due to interactive vegetation cover over North Asia.

INTVEG and NASIAFIX. Heat content variance within the west-central North Pacific is enhanced by up to 35% east of Japan ($p < 0.1$) in INTVEG, which is attributed to remote vegetation feedbacks from northern Asia. The percent variance differences of the following terms (averaged over the top 100 m) are computed: surface heat flux, anomalous advection, mean advection, horizontal diffusion, and vertical diffusion and convection (Wu and Liu 2005). The enhanced ocean heat content variance in INTVEG, compared to NASIAFIX, appears to be largely related to the enhanced variance in anomalous horizontal heat advection [$v'(\partial\overline{T}/\partial y)$ and $u'(\partial\overline{T}/\partial x)$] ($p < 0.1$). Over the Kuroshio Extension, the variance in oceanic meridional currents is enhanced in INTVEG, particularly during MAM and JJA. In MAM, when SST variance over the Kuroshio Extension is most enhanced in INTVEG compared to NASIAFIX, there is a 22% increase in variance in anomalous meridional heat advection over the Kuroshio Extension. These results suggest that vegetation cover variability over northern Asia is impacting the atmospheric circulation pattern, thereby influencing meridional ocean currents and heat transport across the North Pacific. Local surface fluxes of sensible and latent heat are significantly enhanced in INTVEG upstream over the Kuroshio region but not the Kuroshio Extension, suggesting a remote contribution to enhanced Kuroshio Extension SST variability. In agreement with our findings, the dominant influence of meridional heat advection by anomalous ocean currents on SST variability in the Kuroshio Extension has been noted in previous studies (Latif and Barnett 1994, 1996; Seager et al. 2001; Vivier et al. 2002; Wu et al. 2003; Kelly 2004; Kwon and Deser 2007), with local surface fluxes playing less of a role (Kelly 2004).

5. Impact of vegetation variability on the atmosphere

The percent difference in variance of annual surface air temperature is shown between INTVEG and NASIAFIX in Fig. 3a and between NASIAINT and FIXVEG in Fig. 3b. Two connected regions of enhanced temperature variance ($p < 0.1$) are identified in the simulations with interactive northern Asian vegetation: the Kuroshio Extension and northeastern China/Mongolia. Since the mean surface winds are westnorthwesterly over these regions, fluctuations in temperature over northeastern China are likely to impact the Kuroshio Extension through the mean advection of temperature anomalies downstream. Temperature variance is 20% greater ($p < 0.1$) over northeastern China/Mongolia and 25% greater ($p < 0.1$) over the Kuroshio Extension region in INTVEG compared to NASIAFIX. Likewise, the variance is 20% and 35% greater ($p < 0.1$), respectively, in NASIAINT compared to FIXVEG.

Over the Kuroshio Extension, the variance in surface air temperature is 35% greater ($p < 0.1$) for MAM in INTVEG compared to NASIAFIX. Over northeastern China, variance is 25% greater ($p < 0.1$) for September–November (SON) in INTVEG compared to NASIAFIX. These seasonal results qualitatively agree with the comparison of NASIAINT with FIXVEG. Interestingly, the largest differences in temperature variance between simulations are located outside the critical North Asia box, suggesting substantial remote vegetation feedbacks. Similar to studies by Bonan et al. (1995), Chase et al. (2000), Zhao et al. (2001), and Lynch et al. (2003), we found that vegetation changes within the forest–tundra transition region over northern Asia can have significant widespread impacts on climate.

6. Mechanism of remote feedback

Variations in forest cover along the northern boreal forest of Eurasia, which are largely driven by fluctuations in surface radiation (related to cloudiness), produce a local albedo feedback that initiates the remote feedback on Pacific SST. This albedo feedback is the result of the forest canopy masking snow cover or increased energy absorption into the canopy, with an increase in forest cover reducing the albedo (Lynch et al. 2003) and increasing the surface air temperature. Figure 4 presents lead–lag correlations between annual forest cover and seasonal albedo over North Asia (55°–80°N, 50°–140°E) from INTVEG. The instantaneous relationship between annual forest cover and seasonal albedo is most negative ($r = -0.4$) in JJA. However, the vegetation feedback is greatest on MAM albedo, similar to the study by Lynch et al. (2003), and is significant for up to 3–4 yr. This represents the reduction of springtime albedo over the span of several years following an increase in forest cover and masking of snow. Although the correlations with forest cover leading December–February (DJF) albedo are significant out to 3 yr, the minimal amount of solar radiation at the high latitudes likely makes this feedback to climate minimal.

Within the critical North Asian region, variability in forest cover feeds back to the sea level pressure pattern. Anomalously high forest cover fraction over northern Asia results in lower albedo and, thus, higher temperatures, which contribute to a lowering of the atmospheric pressure. In particular, tree cover variations in the western dipole center (60°–70°N, 70°–90°E) affect the October–April (dominant period for Siberian high) sea level pressure downstream, over north-central Asia (55°–80°N, 70°–120°E) (Fig. 5a). Tree cover fractions over northern Asia exhibit a memory of one to two

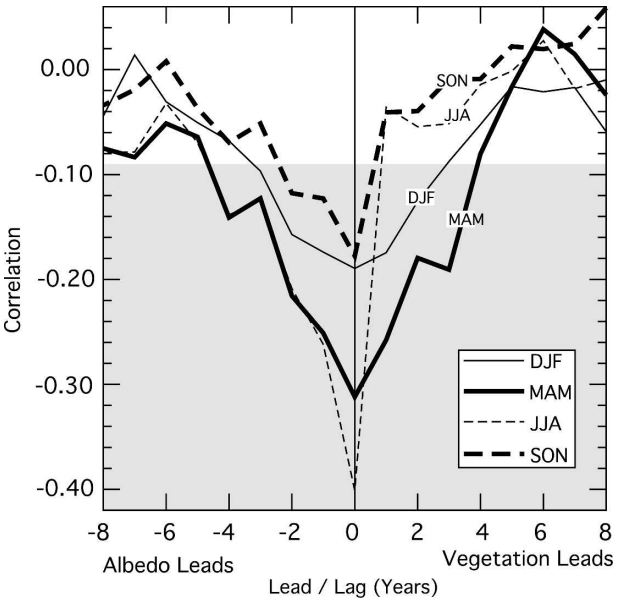

FIG. 4. Lead–lag correlations between annual forest cover fraction and seasonal planetary albedo in North Asia (55°–80°N, 50°–140°E). Correlations are computed with (left) albedo leading forest cover, and (right) forest cover leading albedo. Shading indicates statistical significance at the 90% level. The surface albedo was unfortunately not available for the simulation.

decades, based on the significance (90%) of autocorrelations at different time lags. As a consequence, the atmospheric response to tree cover anomalies can be quite persistent. A period of anomalously high forest cover fraction in the west dipole center is often followed by a significant decrease in sea level pressure during the next 2 to 8 yr over north-central Asia ($p < 0.1$). In spite of being statistically significant, the correlation of annual forest cover against a single year's sea level pressure is not particularly high, because of a strong internal atmospheric variability. However, the long persistence of a positive tree cover anomaly supports a pattern of lower atmospheric pressure over several subsequent years. As shown in Fig. 5b, the correlation between annual forest cover in the west dipole center and October–April sea level pressure averaged over the following 8 yr at all points is most negative ($r < -0.3$) over north-central Russia, just downstream of the west dipole center. The variance in annual sea level pressure over northern Russia is significantly higher (>20%) in INTVEG than NASIAFIX ($p < 0.1$) due to this forest cover–atmospheric circulation relationship. Pressure over the region of the northern Siberian high critically impacts temperature over northern China and, eventually, the Kuroshio Extension. There is a negative correlation between forest cover in the west dipole region and mean October–April surface

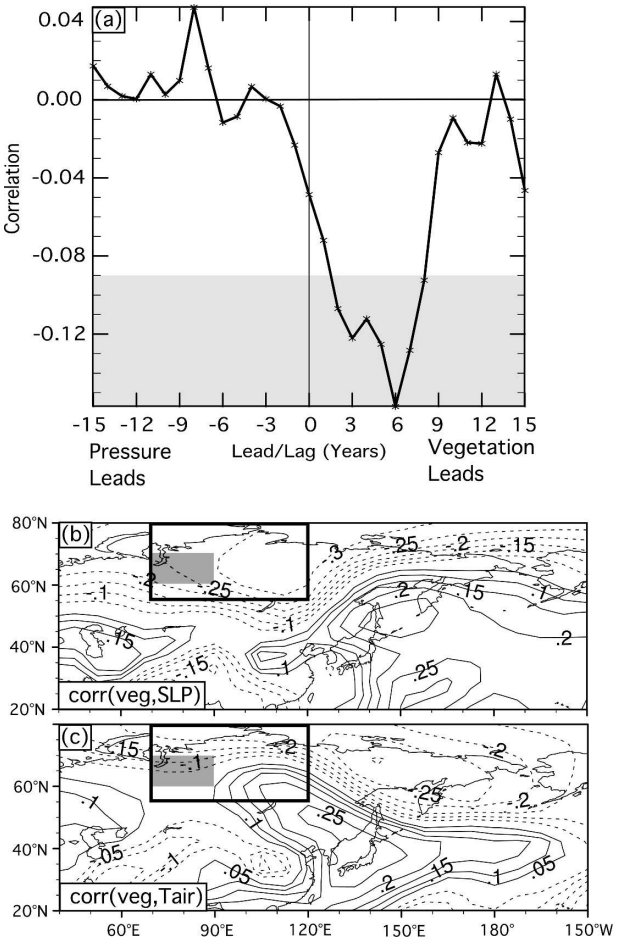

FIG. 5. (a) Lead–lag correlations between annual forest cover fraction in the west dipole center (60°–70°N, 70°–90°E) and October–April sea level pressure over north–central Asia (55°–80°N, 70°–120°E). These two regions are identified in (b) as a shaded box and in (c) as an empty box. Correlations on the right (left) side of (a) represent forest cover (sea level pressure) leading sea level pressure (forest cover). Shading in (a) indicates statistical significance at the 90% level. (b) Correlation between annual forest cover in the west dipole center (gray box) and October–April sea level pressure averaged over the next 8 yr. (c) Correlation between annual forest cover in the west dipole center and October–April surface air temperature averaged over the next 8 yr.

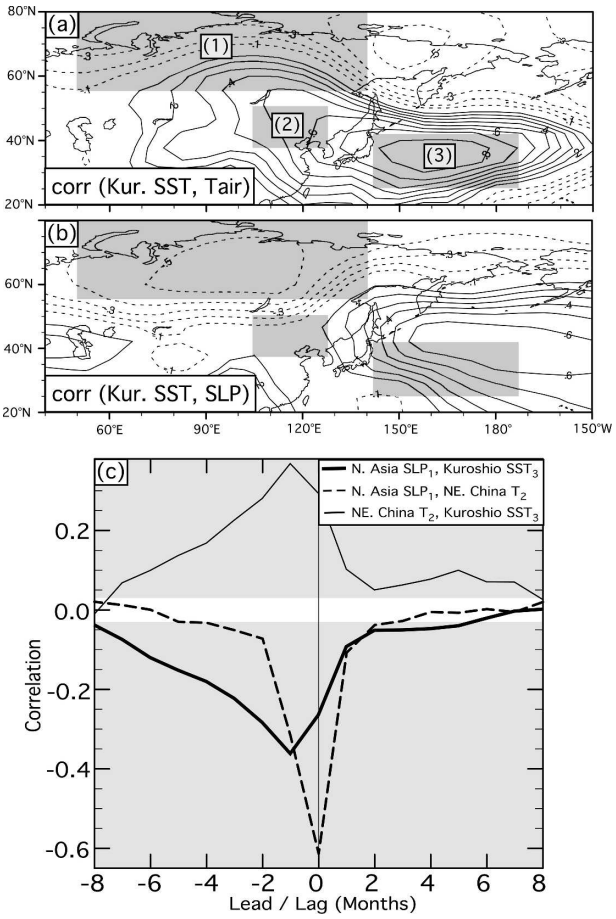

FIG. 6. (a) Instantaneous correlation between annual Kuroshio SST and surface air temperature at all other points in simulation INTVEG. (b) Instantaneous correlation between annual Kuroshio SST and sea level pressure at all other points in INTVEG. In (a) and (b), the shaded boxed represent the Kuroshio Extension, northeast China, and the region with fixed vegetation cover in simulation NASIAFIX. (c) Lead–lag correlations between monthly anomalies of North Asian sea level pressure and Kuroshio SST (thick solid line), North Asian sea level pressure and northeast China's surface air temperature (dashed line), and northeast China's surface air temperature and Kuroshio SST (thin solid line). Correlations on the left side of the plot represent the first named variable leading the second named variable. Shading indicates statistical significance at the 90% level. Subscripts in legend indicate regional boxes in (a).

air temperature averaged over the following 8 yr across a band stretching through eastern Russia, northeastern China, Japan, and the Kuroshio Extension (Fig. 5c). A positive forest cover anomaly over the western dipole center tends to lead to a weaker northern Siberian high, which limits its ability to access Arctic air masses, reduces northerly winds and cold air advection to the east of the high, and results in warmer conditions to the southeast. This establishes a link between the forest cover over northern Asia and temperatures over the Kuroshio Extension.

The link between Kuroshio Extension SSTs and Asian climate variability is further investigated in Fig. 6. Annual Kuroshio Extension SSTs in INTVEG are correlated against surface air temperature and sea level pressure at all points in Figs. 6a,b, respectively. Given a mean west-northwesterly lower-tropospheric wind, temperatures across much of East Asia, particularly northeastern China, are significantly correlated with Kuroshio Extension SSTs (Fig. 6a). Kuroshio Extension SSTs are also found to be significantly anticorre-

lated with sea level pressure over northern Russia (Fig. 6b). The correlation pattern of Fig. 6b closely matches the pattern of EOF-1 for the North Asian annual sea level pressure (41% of the variance). In particular, DJF sea level pressure over northern Russia is highly anticorrelated ($r < -0.4$) with the following MAM Kuroshio Extension SST, suggesting a stronger wintertime northern Siberian high supporting lower springtime Kuroshio Extension SSTs. These findings reflect previous studies using observational data. Panagiotopoulos et al. (2005) noted that the Siberian high's observed impact on atmospheric circulation and temperature extends over a vast area from the Arctic to the tropical Pacific, with the strength of the Siberian high negatively correlated with temperatures over Siberia and extending southeastward to the Kuroshio Extension. Observed changes in sea level pressure anomalies over the northern Siberian high also have a strong influence on the East Asian winter monsoon (Gong et al. 2001), with a stronger high leading to lower SSTs in the Sea of Japan (Minobe et al. 2004).

Monthly lead–lag correlations are performed for the regions of North Asia (55°–80°N, 50°–140°E), northeast China (38°–51°N, 105°–130°E), and the Kuroshio Extension (30°–40°N, 140°E–180°) (Fig. 6c). The strongest negative correlation between North Asia's sea level pressure and northeast China's surface air temperature is instantaneous, with a stronger northern Siberian high encouraging greater northerlies with cold advection across East Asia. Similarly, Gong et al. (2001) determined that China's observed wintertime temperatures are strongly anticorrelated with sea level pressure variations over the Eurasian high latitudes. In fact, the Siberian high accounts for 44% of the total observed wintertime temperature variance of China on average (Gong and Wang 1999). Observations reveal that, during the winter monsoon, the Siberian high produces cold northerly and northwesterly winds across China, the Sea of Japan, and South China Sea (Chu et al. 2001; Gong et al. 2001).

There is a significant positive correlation between northeast China's surface air temperature and Kuroshio Extension SST, particularly with the former variable leading by one month. Northeast China's air temperatures during DJF are particularly well correlated ($r > 0.4$) with the following MAM Kuroshio Extension SSTs. Kuroshio Extension SSTs are significantly affected by East Asian air temperatures over the preceding half year, with the mean winds advecting these anomalies over the North Pacific. Finally, North Asian sea level pressure is negatively correlated with Kuroshio Extension SST, especially when pressure leads by one month. In summary, forest cover anomalies along the north side of the Asian boreal forest lead to changes in albedo, which result in changes in temperature and sea level pressure. This atmospheric circulation response produces changes in air temperature over East Asia that are later advected over the Kuroshio Extension, impacting the SSTs.

The enhanced Kuroshio SST variance in INTVEG compared to NASIAFIX results in a substantial change in variance of the large-scale atmospheric circulation over East Asia and the North Pacific (not shown). The mean annual 250-hPa winds over East Asia in INTVEG are dominated by a strong zonal jet stream across Japan with wind speeds reaching 40 m s^{-1}. The variance in annual wind speed peaks along the north and south sides of this jet core, particularly in the jet exit regions where the variance reaches 6–8 m s^{-1}. The variance in 250-hPa wind speed is enhanced by 20%–30% ($p < 0.1$) along the north and south sides of the upper-level jet in INTVEG compared to NASIAFIX, attributed to remote feedbacks from North Asian vegetation and directly linked to enhanced Kuroshio SST variance. The consequence is greater meridional fluctuations in the position of the East Asian upper-level jet stream, with likely consequences on the circulation pattern across the North Pacific and into North America. In an observational study, Panagiotopoulos et al. (2005) likewise found that the subtropical jet over China and the North Pacific is stronger when the Siberian high is intense. Likewise, Lynch et al. (2003) performed an experiment in which they imposed a poleward expansion of the Asian boreal forest and found that the planetary wave pattern of the NH midlatitudes shifted poleward, illustrating the impact of vegetation on the large-scale circulation pattern.

In comparing MAM 500-hPa height variance between INTVEG and NASIAFIX, we determine that there is a 30% enhancement in height variance over the Bering Sea in INTVEG, likely related to sea ice feedbacks, and a slight southward shift of the North Pacific storm track, related to slightly lower mean temperatures over northern Asia and the North Pacific. There is up to a 20% reduction in MAM sea level pressure variance over the Aleutian low in INTVEG.

7. Conclusions

Four simulations, using a fully coupled climate model with dynamic vegetation, FOAM-LPJ, are produced and analyzed to assess potential remote impacts of vegetation variability on SST variability. The most substantial area of forest cover variability is simulated over North Asia, on the poleward side of the boreal forest, dominated by an east–west dipole pattern of forest

cover variability. By comparing the simulations INTVEG with NASIAFIX, and NASIAINT with FIXVEG, the impact of vegetation variability over the northern edge of the Asian boreal forest is isolated. Both comparisons show a robust signal of significantly enhanced Kuroshio Extension SST variance (+30%) when annual vegetation cover is permitted to vary over north-central Russia. Likewise, surface air temperature variance is enhanced in the INTVEG and NASIAINT simulations over the Kuroshio Extension and northeastern China/Mongolia. A mechanism for the enhanced variance is identified. Positive forest cover anomalies over the western dipole region of northern Russia, which tend to persist for years, reduce the albedo by absorbing more radiation in the canopy and masking underlying snow cover. This lower albedo results in higher surface air temperatures and, eventually, lower pressure along the northern Siberian high, which reduces northerly winds and cold advection over northeast Asia. The mean winds then advect warm anomalies over northeast China east-southeastward to the Kuroshio Extension. Thus, the atmosphere serves as a bridge between vegetation variability over North Asia and SST variability over the North Pacific to compose a remote vegetation feedback.

While the lack of observational data of annual forest cover fraction makes it difficult to confirm these model findings, there are several reasons to have confidence in the results, at least qualitatively. Both observed fractional vegetation cover (FVC) data and model output show relatively high variability in total vegetation cover on the poleward side of the Eurasian boreal forest, although the model's variance appears to be too large. Using FOAM-LPJ, Notaro et al. (2005) simulated a poleward shift of the Eurasian boreal forest due to recent increases in atmospheric CO_2, which agreed with satellite data during the past two decades. The model simulates a reasonable PDO pattern, both spatially and temporally. The simulated relationship between the Siberian high and East Asian temperatures agrees well with observed studies.

Acknowledgments. The authors are grateful to Dr. Xubin Zeng for providing the satellite-based fractional vegetation cover data. We thank Professor John Kutzbach, Dr. Sam Levis, Mark Marohl, and two anonymous reviewers for their helpful comments and Dr. Robert Gallimore for the use of two of his simulations. We appreciate the computer resources provided by NCAR. This work was supported by funding from the U.S. Department of Education (DOE), National Oceanic and Atmospheric Administration (NOAA), and National Science Foundation (NSF).

REFERENCES

Beringer, J., F. S. Chapin, C. C. Thompson, and A. D. McGuire, 2005: Surface energy exchanges along a tundra-forest transition and feedbacks to climate. *Agric. For. Meteor.,* **131,** 143–161.

Betts, A. K., and J. H. Ball, 1997: Albedo over the boreal forest. *J. Geophys. Res.,* **102,** 28 901–28 909.

Bonan, G. B., 2002: *Ecological Climatology: Concepts and Applications*. Cambridge University Press, 678 pp.

——, D. Pollard, and S. L. Thompson, 1992: Effects of boreal forest vegetation on global climate. *Nature,* **359,** 716–718.

——, F. S. Chapin III, and S. L. Thompson, 1995: Boreal forest and tundra ecosystems as components of the climate system. *Climatic Change,* **29,** 145–167.

——, S. Levis, S. Sitch, M. Vertenstein, and K. W. Oleson, 2003: A dynamic global vegetation model for use with climate models: Concepts and description of simulated vegetation dynamics. *Global Change Biol.,* **9,** 1543–1566.

Bowers, J. D., and W. G. Bailey, 1989: Summer energy balance regimes for alpine tundra, Plateau Mountain, Alberta, Canada. *Arct. Alp. Res.,* **21,** 135–143.

Chapin, F. S., W. Eugster, J. P. McFadden, A. H. Lynch, and D. A. Walker, 2000: Summer differences among arctic ecosystems in regional climate forcing. *J. Climate,* **13,** 2002–2010.

Chase, T. N., R. A. Pielke, T. G. F. Kittel, R. R. Nemani, and S. W. Running, 2000: Simulated impacts of historical land cover changes on global climate in northern winter. *Climate Dyn.,* **16,** 93–105.

Chu, P. C., J. Lan, and C. Fan, 2001: Japan Sea thermohaline structure and circulation. Part I: Climatology. *J. Phys. Oceanogr.,* **31,** 244–271.

Cramer, B. A., and Coauthors, 2001: Global response of terrestrial ecosystem structure and function to CO_2 and climate change: Results from six dynamic global vegetation models. *Global Change Biol.,* **7,** 357–373.

DeFries, R. S., J. R. G. Townshend, and M. C. Hansen, 1999: Continuous fields of vegetation characteristics at the global scale at 1-km resolution. *J. Geophys. Res.,* **104,** 16 911–16 925.

——, M. C. Hansen, J. R. G. Townshend, A. C. Janetos, and T. R. Loveland, 2000: A new global 1-km dataset of percentage tree cover derived from remote sensing. *Global Change Biol.,* **6,** 247–254.

Delire, C., J. A. Foley, and S. Thompson, 2004: Long-term variability in a coupled atmosphere–biosphere model. *J. Climate,* **17,** 3947–3959.

Drake, J., I. Foster, J. Michalakes, B. Toonen, and P. Worley, 1995: Design and performance of a scalable parallel community climate model. *Parallel Comput.,* **21,** 1571–1591.

Gallimore, R., R. Jacob, and J. Kutzbach, 2005: Coupled atmosphere–ocean–vegetation simulations for modern and mid-Holocene climates: Role of extratropical vegetation cover feedbacks. *Climate Dyn.,* **25,** 755–776.

Gong, D. Y., and S. W. Wang, 1999: Long-term variability of the Siberian High and the possible influence of global warming. *Acta Geogr. Sin.,* **54,** 125–133.

——, ——, and J.-H. Zhu, 2001: East Asian winter monsoon and Arctic Oscillation. *Geophys. Res. Lett.,* **28,** 2073–2076.

Isard, S. A., and M. J. Belding, 1989: Evapotranspiration from the alpine tundra of Colorado, U.S.A. *Arct. Alp. Res.,* **21,** 71–82.

Jacob, R. L., 1997: Low frequency variability in a simulated at-

mosphere ocean system. Ph.D. thesis, University of Wisconsin—Madison, 159 pp.

Kaplan, A., M. Cane, Y. Kushnir, A. Clement, M. Blumenthal, and B. Rajagopalan, 1998: Analyses of global sea surface temperature 1856-1991. *J. Geophys. Res.,* **103,** 18 567–18 589.

Kelly, K. A., 2004: The relationship between oceanic heat transport and surface fluxes in the western North Pacific: 1970–2000. *J. Climate,* **17,** 573–588.

Kiehl, J. T., J. J. Hack, G. B. Bonan, B. A. Boville, D. L. Williamson, and P. J. Rasch, 1998: The National Center for Atmospheric Research Community Climate Model: CCM3. *J. Climate,* **11,** 1131–1150.

Kwon, Y.-O., and C. Deser, 2007: North Pacific decadal variability in the Community Climate System Model version 2. *J. Climate,* in press.

Lafleur, P. M., and W. R. Rouse, 1995: Energy partitioning at treeline forest and tundra sites and its sensitivity to climate change. *Atmos.–Ocean,* **33,** 121–133.

Latif, M., and T. P. Barnett, 1994: Causes of decadal climate variability over the North Pacific and North America. *Science,* **206,** 634–637.

——, and ——, 1996: Decadal climate variability over the North Pacific and North America: Dynamics and predictability. *J. Climate,* **9,** 2407–2423.

Liu, Z., and L. Wu, 2004: Atmospheric response to North Pacific SST: The role of ocean–atmosphere coupling. *J. Climate,* **17,** 1859–1882.

——, J. Kutzbach, and L. Wu, 2000: Modeling climate shift of El Niño in the Holocene. *Geophys. Res. Lett.,* **27,** 2265–2268.

——, B. Otto-Bliesner, J. Kutzbach, L. Li, and C. Shields, 2003: Coupled climate simulation of the evolution of global monsoons in the Holocene. *J. Climate,* **16,** 2472–2490.

——, M. Notaro, J. Kutzbach, and N. Liu, 2006: Assessing global vegetation–climate feedbacks from observations. *J. Climate,* **19,** 787–814.

Lloyd, A. H., 2005: Ecological histories from Alaskan tree lines provide insight into future change. *Ecology,* **86,** 1687–1695.

Lundberg, A., and J. Beringer, 2005: Albedo and snowmelt rates across a tundra-to-forest transition. Preprints, *15th Int. Northern Research Basins Symp. and Workshop,* Luleä to Kvikkjokk, Sweden, Lund University, 10 pp.

Lynch, A. H., A. R. Rivers, and P. J. Bartlein, 2003: An assessment of the influence of land cover uncertainties on the simulation of global climate in the early Holocene. *Climate Dyn.,* **21,** 241–256.

Mantua, N. J., S. R. Hare, Y. Zhang, J. M. Wallace, and R. C. Francis, 1997: A Pacific interdecadal climate oscillation with impacts on salmon production. *Bull. Amer. Meteor. Soc.,* **78,** 1069–1079.

McFadden, J. P., 1998: The effects of plant growth forms on the surface energy balance and moisture exchange of Arctic tundra. Ph.D. dissertation, University of California, Berkeley, 123 pp. [Available from UMI Dissertation Services, 200 N. Zeeb Road, Ann Arbor, MI 48106-1346.]

McGuire, A. D., and Coauthors, 2001: Carbon balance of the terrestrial biosphere in the twentieth century: Analyses of CO_2, climate and land use effects with four process-based ecosystem models. *Global Biogeochem. Cycles,* **15,** 183–206.

Miller, A. J., D. R. Cayan, and W. B. White, 1998: A westward-intensified decadal change in the North Pacific thermocline and gyre-scale circulation. *J. Climate,* **11,** 3112–3127.

Minobe, S., A. Sako, and M. Nakamura, 2004: Interannual to interdecadal variability in the Japan Sea based on a new gridded upper water temperature dataset. *J. Phys. Oceanogr.,* **34,** 2382–2397.

Notaro, M., Z. Liu, R. Gallimore, S. J. Vavrus, J. E. Kutzbach, I. C. Prentice, and R. L. Jacob, 2005: Simulated and observed preindustrial to modern vegetation and climate changes. *J. Climate,* **18,** 3650–3671.

——, ——, and J. W. Williams, 2006: Observed vegetation–climate feedbacks in the United States. *J. Climate,* **19,** 763–786.

——, S. Vavrus, and Z. Liu, 2007: Global vegetation and climate change due to future increases in CO_2 as projected by a fully coupled model with dynamic vegetation. *J. Climate,* **20,** 70–90.

Panagiotopoulos, F., M. Shahgedanova, A. Hannachi, and D. B. Stephenson, 2005: Observed trends and teleconnections of the Siberian High: A recently declining center of action. *J. Climate,* **18,** 1411–1422.

Parker, D. E., P. D. Jones, C. K. Folland, and A. Bevan, 1994: Interdecadal changes of surface temperature since the late nineteenth century. *J. Geophys. Res.,* **99,** 14 373–14 399.

Reynolds, R. W., and T. M. Smith, 1994: Improved global sea surface temperature analyses. *J. Climate,* **7,** 929–948.

Riseborough, D. W., and C. A. Burn, 1988: Influence of an organic mat on the active layer. *Proc. Fifth Int. Conf. on Permafrost,* Trongheim, Norway, Tapir Publications, 633–638.

Robinson, D. A., and G. Kukla, 1985: Maximum surface albedo of seasonally snow-covered lands in the Northern Hemisphere. *J. Climate Appl. Meteor.,* **24,** 402–411.

Rouse, W. R., D. W. Carlson, and E. J. Weick, 1992: Impacts of summer warming on the energy and water balance of wetland tundra. *Climatic Change,* **22,** 305–326.

Seager, R., Y. Kushnir, N. Naik, M. A. Cane, and J. A. Miller, 2001: Wind-driven shifts in the latitude of the Kuroshio–Oyashio Extension and generation of SST anomalies on decadal timescales. *J. Climate,* **14,** 4249–4265.

Shaeffer, J. D., and E. R. Reiter, 1987: Measurements of surface energy budgets in the Rocky Mountains of Colorado. *J. Geophys. Res.,* **92,** 4145–4162.

Sitch, S., 2000: The role of vegetation dynamics in the control of atmospheric CO_2 content. Ph.D. dissertation, Lund University, 213 pp.

——, and Coauthors, 2003: Evaluation of ecosystem dynamics, plant geography and terrestrial carbon cycling in the LPJ dynamic global vegetation model. *Global Change Biol.,* **9,** 161–185.

Smith, T. M., and R. W. Reynolds, 2003: Extended reconstruction of global sea surface temperatures based on COADS data (1854–1997). *J. Climate,* **16,** 1495–1510.

——, and ——, 2004: Improved extended reconstruction of SST (1854–1997). *J. Climate,* **17,** 2466–2477.

Snyder, P. K., C. Delire, and J. A. Foley, 2004: Evaluating the influence of different vegetation biomes on the global climate. *Climate Dyn.,* **23,** 279–302.

Sturm, M., J. P. McFadden, G. E. Liston, F. S. Chapin III, C. H. Racine, and J. Holmgren, 2001: Snow–shrub interactions in Arctic tundra: A hypothesis with climatic implications. *J. Climate,* **14,** 336–344.

Vivier, F., K. A. Kelly, and L. Thompson, 2002: Heat budget in the Kuroshio Extension region: 1993–99. *J. Phys. Oceanogr.,* **32,** 3436–3454.

Wohlfahrt, J., S. P. Harrison, and P. Braconnot, 2004: Synergistic feedbacks between ocean and vegetation on mid- and high-

latitude climates during the mid-Holocene. *Climate Dyn.,* **22,** 223–238.

Wu, L., and Z. Liu, 2002: Is tropical Atlantic variability driven by the North Atlantic Oscillation? *Geophys. Res. Lett.,* **29,** 1653, doi:10.1029/2002GL014939.

——, and ——, 2003: Decadal variability in the North Pacific: The eastern North Pacific mode. *J. Climate,* **16,** 3111–3131.

——, and ——, 2005: North Atlantic decadal variability: Air–sea coupling, oceanic memory, and potential Northern Hemisphere resonance. *J. Climate,* **18,** 331–349.

——, ——, and R. Gallimore, 2003: Pacific decadal variability: The tropical Pacific mode and North Pacific mode. *J. Climate,* **16,** 1101–1120.

Xie, S.-P., T. Kunitani, A. Kubokawa, M. Nonaka, and S. Hosoda, 2000: Interdecadal thermocline variability in the North Pacific for 1958–97: A GCM simulation. *J. Phys. Oceanogr.,* **30,** 2798–2813.

Zeng, N., and J. D. Neelin, 2000: The role of vegetation–climate interaction and interannual variability in shaping the African savanna. *J. Climate,* **13,** 2665–2670.

——, ——, K.-M. Lau, and C. J. Tucker, 1999: Enhancement of interdecadal climate variability in the Sahel by vegetation interaction. *Science,* **286,** 1537–1540.

——, K. Hales, and J. D. Neelin, 2002: Nonlinear dynamics in a coupled vegetation–atmosphere system and implications for desert–forest gradient. *J. Climate,* **15,** 3474–3487.

Zeng, X., R. E. Dickinson, A. Walker, M. Shaikh, R. S. DeFries, and J. Qi, 2000: Derivation and evaluation of global 1-km fractional vegetation cover data for land modeling. *J. Appl. Meteor.,* **39,** 826–839.

Zhao, M., A. J. Pitman, and T. Chase, 2001: The impact of land cover change on the atmospheric circulation. *Climate Dyn.,* **17,** 467–477.